frontiers in Electronics

ORIGINAL RESEARCH
published: 09 December 2021
doi: 10.3389/felec.2021.797308

Mechanical Stress Stability of Flexible Amorphous Zinc Tin Oxide Thin-Film Transistors

Oliver Lahr, Max Steudel, Holger von Wenckstern and Marius Grundmann*

Felix Bloch Institute for Solid State Physics, Universität Leipzig, Leipzig, Germany

Due to their low-temperature processing capability and ionic bonding configuration, amorphous oxide semiconductors (AOS) are well suited for applications within future mechanically flexible electronics. Over the past couple of years, amorphous zinc tin oxide (ZTO) has been proposed as indium and gallium-free and thus more sustainable alternative to the widely deployed indium gallium zinc oxide (IGZO). The present study specifically focuses on the strain-dependence of elastic and electrical properties of amorphous zinc tin oxide thin-films sputtered at room temperature. Corresponding MESFETs have been compared regarding their operation stability under mechanical bending for radii ranging from 5 to 2 mm. Force-spectroscopic measurements yield a plastic deformation of ZTO as soon as the bending-induced strain exceeds 0.83 %. However, the electrical properties of ZTO determined by Hall effect measurements at room temperature are demonstrated to be unaffected by residual compressive and tensile strain up to 1.24 %. Even for the maximum investigated tensile strain of 1.26 %, the MESFETs exhibit a reasonably consistent performance in terms of current on/off ratios between six and seven orders of magnitude, a subthreshold swing around 350 mV/dec and a field-effect mobility as high as 7.5 $cm^2V^{-1}s^{-1}$. Upon gradually subjecting the transistors to higher tensile strain, the channel conductivity steadily improves and consequently, the field-effect mobility increases by nearly 80 % while bending the devices around a radius of 2 mm. Further, a reversible threshold voltage shift of about −150 mV with increasing strain is observable. Overall, amorphous ZTO provides reasonably stable electrical properties and device performance for bending-induced tensile strain up to at least 1.26 % and thus represent a promising material of choice considering novel bendable and transparent electronics.

Keywords: zinc tin oxide, amorphous oxide semiconductor, flexible electronics, transparent electronics, sustainable, abundant, MESFETs, thin-film transistors

OPEN ACCESS

Edited by:
Luisa Petti,
Free University of Bozen-Bolzano, Italy

Reviewed by:
Devendra Singh,
Ulsan National Institute of Science and Technology, South Korea
Stefano Lai,
University of Cagliari, Italy

****Correspondence:***
Oliver Lahr
oliver.lahr@physik.uni-leipzig.de

Specialty section:
This article was submitted to Flexible Electronics, a section of the journal Frontiers in Electronics

Received: *18 October 2021*
Accepted: *08 November 2021*
Published: *09 December 2021*

Citation:
Lahr O, Steudel M, von Wenckstern H and Grundmann M (2021) Mechanical Stress Stability of Flexible Amorphous Zinc Tin Oxide Thin-Film Transistors. Front. Electron. 2:797308. doi: 10.3389/felec.2021.797308

1 INTRODUCTION

With the rapid evolution of active-matrix flat-panel display technology, significantly advanced by the replacement of commonly deployed silicon by indium gallium zinc oxide (IGZO) approximately a decade ago, amorphous oxide semiconductors (AOS) have considerably gained interest leading to the development of a distinct, thriving research area (Hosono, 2018). The continuously growing demand for scalable electronics, requiring low power consumption and high-frequency operation capability, however, has triggered recent efforts to substitute scarce materials such as IGZO by

compounds comprising earth-abundant elements only. Amorphous zinc tin oxide (ZTO) represents such a viable choice regarding a more sustainable and cost-efficient approach to transparent as well as bendable electronics, attributed to the possibility of room-temperature fabrication combined with its reasonably high charge carrier mobility exceeding $10\,cm^2V^{-1}s^{-1}$ for thin-films deposited at room temperature (Schlupp et al., 2013).

Even though ZTO appears to be a suitable candidate for use in flexible device building blocks, the vast majority of previously published issues covering ZTO based devices primarily report metal-insulator field-effect transistors (MISFETs) fabricated on rigid substrates. Only a few flexible devices implementing ZTO have so far been demonstrated, including MISFETs fabricated between 180°C and 300 °C and junction field-effect transistor (JFET) based inverters (Jackson et al., 2005; Jackson et al., 2006; Fernandes et al., 2018; Lee et al., 2018; Schlupp et al., 2020). Over the past couple of years, JFET and especially metal-semiconductor field-effect transistor (MESFET) technology has proven to be a viable approach to obtain high-performance ZTO based electronics providing both low-power operation and fabrication at room temperature (Dang et al., 2017; Vogt et al., 2018; Lahr et al., 2019a; Lahr et al., 2020a). Further, the successful implementation of amorphous ZTO within integrated circuits such as logic inverters and ring oscillators yielded a remarkable voltage gain as high as 1190 as well as single stage delay times as low as 277 ns, respectively, rendering amorphous ZTO a reasonable competitor within the scope of future AOS based electronic applications (Lahr et al., 2019b; Lahr et al., 2020b).

This study focuses on evaluating the effect of bending-induced strain on the properties of amorphous ZTO thin-films as well as the limits to excessive bending stress on the performance of ZTO based MESFETs. Performing force-distance measurements with bent samples enabled the *in-situ* investigation of the elastic behavior of ZTO in dependence on the induced strain. Additionally, the effect of residual compressive and tensile strain on the electrical properties of ZTO thin-films has been determined by Hall effect and conductivity measurements at room temperature, while the sample was subjected to bending-induced mechanical stress in between measurements. Finally, the performance of ZTO/PtO_x based MESFETs and associated transistor parameters have been studied regarding their stability under tensile strain up to $\varepsilon = 1.26\,\%$, corresponding to a bending radius of 2 mm.

2 MATERIALS AND METHODS

ZTO thin-films with a cation composition ratio of 1:1 Zn:Sn have been deposited by RF magnetron sputtering on 50 μm thick polyimide substrates using a single ceramic target. To maintain compatibility with the limited thermal stability of common organic substrates, the deposition temperature has been restricted to room temperature while the processing temperatures associated with photoresist developing during photolithographic patterning did not exceed 110 °C. Prior device fabrication, 50 µm thick polyimide substrates (DUPONT KAPTON E and KOLON CPI) were preshrunk under vacuum atmosphere at 200 °C for 24 h and have then been sonicated in acetone and isopropanol (Münzenrieder et al., 2011). Photolithographic patterning has been performed using a HEIDELBERG µMLA direct laser writing lithography system with AZ 1514H photoresist and AZ 351B developer (both from MICROCHEMICALS), followed by a conventional ultrasonic lift-off process using N-methyl-2-pyrrolidon.

The ZTO sputtering process has been ignited in oxygen-rich atmosphere to grow a 10 nm thin intrinsic layer (*i*-ZTO) underneath the conductive *n*-ZTO channel in order to compensate electron accumulation at the interface by inducing oxygen incorporation and thus enabling sufficient channel depletion (Vogt et al., 2018). Ohmic source and drain contacts consist of 30 nm DC sputtered Au. MESFET gates have been deposited in a single final step, comprising 10 nm *i*-ZTO as well as 150 nm PtO_x capped with 30 nm Pt. Again, the thin semi-insulating *i*-ZTO layer between channel and gate significantly improves the device performance in terms of reducing the gate leakage current by saturating under-coordinated cation bonds due to oxygen transfer in the vicinity of the channel surface. Despite being intrinsically undoped and thus way less conductive $\rho > 10^3\,\Omega m$), the *i*-ZTO layer, however, does not induce a conduction band offset. In fact, the ZTO/*i*-ZTO contact forms rather an n/n^- type of junction with decreasing net doping density toward the metal interface. Previous investigations of corresponding Schottky barrier diodes yield the effective barrier height to be independence of *i*-ZTO being embedded between ZTO and PtO_x (Schlupp et al., 2015; Schlupp et al., 2017).

Electrical properties of ZTO thin-films have been determined by Hall effect measurements at room temperature. Static current-voltage measurements were recorded using a SÜSS P200 wafer prober system and a LAKESHORE MODEL 8425 probe station each connected to an AGILENT 4155C semiconductor parameter analyzer. Force spectroscopy have been performed with a PARK SCIENTIFIC XE150 atomic force microscopy (AFM) system using a DD-ACTA Si probe coated with polycrystalline boron-doped diamond (spring constant $40\,Nm^{-1}$, tip radius < 150 nm). Amorphous growth and the thickness of ZTO has been confirmed by X-ray diffraction and X-ray reflectivity measurements, respectively.The minimum bending-induced strain

$$\varepsilon = \frac{z - z_{neutral}}{R} \tag{1}$$

for corresponding radii R has been calculated by estimating the location of the neutral plane $z_{neutral}$ within the entire material stack of height z (Heremans et al., 2016). $z_{neutral}$ takes into account the individual thickness of constituent layers as well as their corresponding approximate Young's modulus of 2.8, 110, 60, 126 and 140 GPa for polyimide, ZTO, Au, PtO_x and Pt, respectively (Salvadori et al., 2003; Jain et al., 2013). In the following, the neutral plane has been assumed to be constant throughout the sample, even though its position slightly shifts across the sample plane due to the lateral thickness differences of the investigated devices. Further, **Eq. 1** neglects the residual strain - remaining from previous bending events - within the constituent device layers (Townsend et al., 1987).

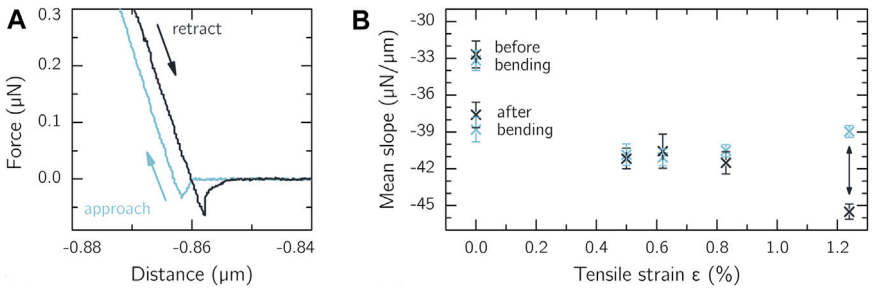

FIGURE 1 | (A) Exemplary force-distance characteristic acquired by force spectroscopy via AFM of an unbent ($\varepsilon = 0\,\%$) amorphous 24 nm thick ZTO thin-film sample grown on a flexible polyimide substrate, indicating an elastic deformation behavior **(B)** Tensile-strain-dependent mean slopes derived from the approaching and retracting curves of eight separately performed force-distance measurements per bending radius across the ZTO sample. ε has been calculated according to **Eq. 1** for bending radii ranging from 5 mm down to 2 mm.

3 RESULTS AND DISCUSSION

3.1 Elasticity of Amorphous ZTO

In order to investigate the impact of bending induced strain on the mechanical properties of amorphous ZTO, force-distance curves of 24 nm thick ZTO thin-films, deposited on polyimide substrates, have been recorded via force spectroscopy using AFM to monitor the tip-sample interactions via perpendicular cantilever deflection. Respective exemplary force-distance curves of ZTO are depicted in **Figure 1A**. While the cantilever approaches the sample down to a few nanometers of separation between tip and surface, the prevailing attractive van der Waals forces cause the tip to snap into contact, as indicated by the observed minimum of the effective force. Once the tip is in close contact with the thin-film, repulsive Pauli interaction dominates the observed characteristic of the approaching curve, as the scanner further extends toward the sample. At a certain predetermined force setpoint, the scanner starts to retract the tip from the sample. Consequently, the cantilever will bend toward the surface due to attractive adhesive forces, given by the second observed minimum in **Figure 1A**. During further withdrawal of the scanner, the tip detaches from the surface as the elastic constant of the cantilever overcomes the adhesive forces between tip and sample (Cappella and Dietler, 1999).

Figure 1B depicts the strain-dependence of the mean slopes - determined for both the approaching and retraction curves - out of eight force-distance measurement points per bending radius equally distributed across a sample area of 1 μm^2. Starting with the unbent state $\varepsilon = 0\,\%$, the investigated bending radii have been gradually reduced from $R = 5$ mm down to $R = 2$ mm in steps of 1 mm, corresponding to a tensile strain of 0.5 % up to 1.24 %, respectively. By subjecting the sample to a strain up to $\varepsilon \leq 0.83\,\%$, the resulting higher steepness of the mean slopes clearly suggests an increased stiffness of ZTO. Comparing the slope after the bending procedures with the initial measurement, the sample maintains its slightly higher stiffness, which is probably attributed to residual strain effects and the ZTO thin-film not being fully relaxed during the repeated measurement in its unbent state. The strain-independence of the slopes up to a bending radius of 3 mm, regardless of the scanning-direction, indicates only an elastic deformation of the ZTO thin-film. Further increasing the tensile strain beyond 0.83 %, results in a plastic deformation, since both slopes deviate considerably. ZTO starts to become softer as the tip advances further into the sample, given by the decreased slope of the approaching curve. The absolute value of the mean slope of the retraction curve, however, increases significantly due to compression of the surface by the cantilever tip, causing the thin-film to deform irreversibly. Comparing the mean slopes before and after the bending procedure suggests that the total stress exerted on ZTO causes a substantial amount residual strain to remain in the thin-film. Note that the observed plastic deformation results from combined tensile strain and probing-induced stress; thus the ZTO thin-film might not necessarily undergo plastic deformation across the whole sample but rather in the vicinity of the measurement points.

Figure 2A depicts the exerted probing stress in terms of the attractive tip-sample pull-on force as well as the corresponding adhesion force, calculated for a tip contact area of approximately $7 \times 10^{-14}\,m^2$ and the maximum adhesive force given by the minima of the approaching and retraction curve, respectively. Both stresses appear to be strain-independent and are rather determined by thin-film material itself, as further verified by comparing the initial results with a repeated measurement for the unbent case in **Figure 2B**, after the sample has been exposed to mechanical bending stress. Hence, the force exerted on the sample surface by the cantilever was approximately the same for all measurements. A similar adhesive tip-sample relationship has also been observed regardless whether the ZTO thin-film has been deposited on polyimide or on a quartz glass substrate.

3.2 Strain-Dependence of Electrical Properties

Conductivity as well as Hall effect measurements based on the van der Pauw configuration have been performed at room temperature to gain further insight to what extent bending-induced residual strain affects the electrical properties of amorphous ZTO thin-films. Therefor, 14 nm of ZTO were grown on two $10 \times 10\,mm^2$ polyimide substrates, exhibiting a resistivity of $2 \times 10^{-3}\,\Omega m$, a free-carrier concentration of $4 \times 10^{18}\,cm^{-3}$ and a charge-carrier mobility of $7.2\,cm^2V^{-1}s^{-1}$. Both samples have then been subjected to either compressive or tensile

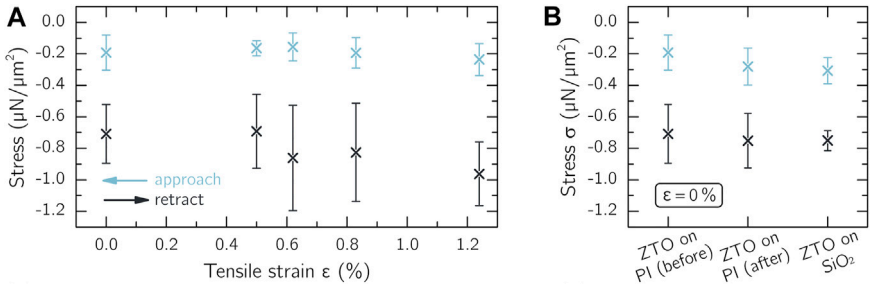

FIGURE 2 | (A) Strain-dependence of the mechanical stress exerted on the ZTO thin-film by the cantilever tip in terms of attractive pull-on force (snap-in) as well as adhesion force per cantilever tip area of $7{\cdot}10^{-14}\,m2$ during the force-distance measurements **(B)** Comparison of the stress exerted by the cantilever tip on ZTO thin-films deposited on quartz glass as well as on polyimide (PI) substrates before and after the bending the sample (ε = 0 %).

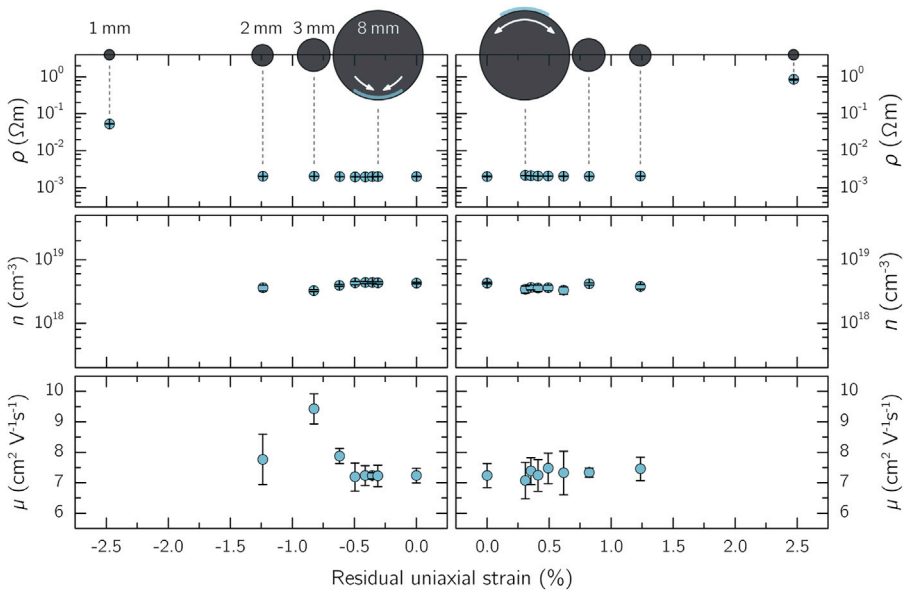

FIGURE 3 | Resistivity, free-carrier concentration and charge-carrier mobility of amorphous ZTO thin-films as a function on the residual compressive and tensile strain, remaining in the sample upon bending to radii ranging from 8 mm down to 1 mm. Beyond ε =±1.24 %, the Hall effect results were not clearly evaluable due to alternating signs of the Hall coefficients.

bending for 10 s in between measurements, while the radius was gradually reduced from 8 to 1 mm. A side-by-side comparison of associated electrical thin-film properties is given in **Figure 3**. Overall, the vast majority of the obtained electrical properties are unaffected by the residual strain regardless of the chosen bending radius between 8 and 2 mm. The duration of each Hall measurement of about 15 min per bending cycle appears to be sufficiently enough relaxation time for the ZTO thin-film to compensate possible effects of residual strain. An increased charge-carrier mobility from approximately $8\,cm^2V^{-1}s^{-1}$–$9.5\,cm^2V^{-1}s^{-1}$ is observable for compressive strain of −0.83 % and presumably associated with the remaining influence of residual strain in the ZTO layer. However, as the mobility decreases to its initial value for ε = − 1.24 %, these changes turn out to be reversible.

For strain exceeding ±1.24 %, only resistivity data are shown, since the corresponding Hall effect results are not clearly evaluable due to alternating signs of the Hall coefficients. As soon as the strain approaches ε = ± 2.5 %, a significant increase of the resistivity of up to more than two order of magnitude is notable for both compressive and tensile strain, which is most likely associated with the ZTO surface starting to become brittle. Consequently, bending the sample around 1 mm causes the surface to be permanently damaged, resulting in irreversible changes of the electrical properties. Note that Hall effect measurements are generally very sensitive to disturbances of the thin-film homogeneity and excessive bending the sample eventually causes the polyimide substrate to plastically deform as well by and to maintain its bent shape which might affect the measurement in general regardless of the condition of ZTO layer. A direct comparison between the impact of excessive compressive and tensile strain, being responsible for plastic deformation, yields a much more pronounced effect of the tensile strain on

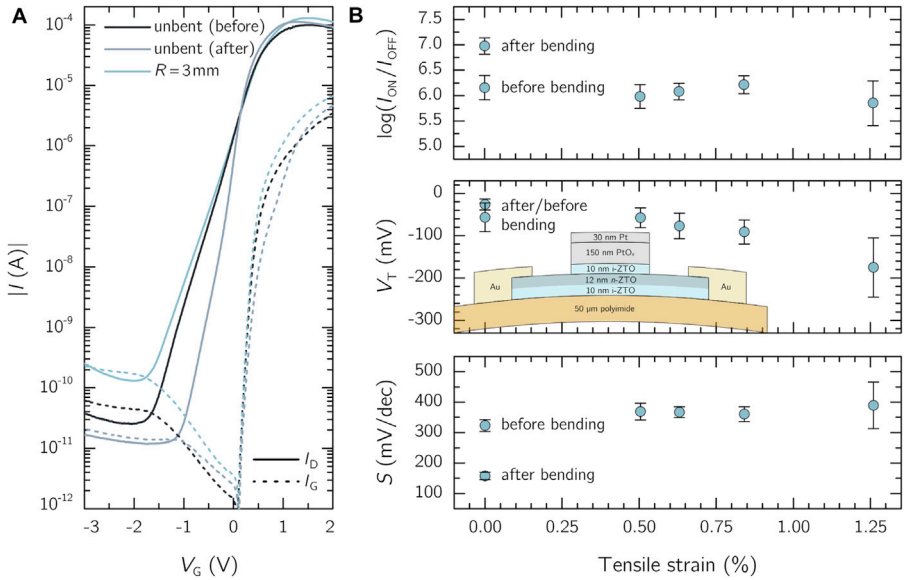

FIGURE 4 | (A) Exemplary static transfer characteristics and associated gate leakage current of a ZTO/PtO_x based MESFET recorded for a bending radius of 3 mm as well as before and after the bending procedures including radii ranging from 5 mm down to 2 mm.The strain has been applied parallel to the channel, i.e., to the current flow direction. The source-drain voltage was fixed at 2 V and the gate width and length are 200 µm and 2 µm, respectively. For better clarity, only the scanning direction from positive to negative gates voltages are shown **(B)** Strain-dependence of the associated current on/off ratio, subthreshold swing and threshold voltage, determined from transfer characteristics of ZTO based MESFETs. For ε =0 %, the transistor parameters before and after the whole bending procedure are depicted. The inset schematically depicts the basic material stacking order of a MESFET with corresponding layer thicknesses.

the overall condition of the surface and thus the electrical properties of the ZTO thin-film. Similar observations have been made for flexible IGZO based transistors, where the device performance is usually more affected by bending-induced tensile strain (Heremans et al., 2016; Billah et al., 2017).

3.3 Performance Durability of Flexible ZTO Based Devices

Static current transfer characteristics of a typical ZTO/PtO_x based MESFET are depicted in **Figure 4A**, recorded for various bending radii ranging from 5 to 2 mm and with a fixed source-drain voltage of 2 V. Corresponding strain values have been calculated by estimating the location of the neutral plane along the gate-channel layer stack according to **Eq. 1**. However, note that the overall induced strain within the ZTO channel is larger at the uncovered parts of the channel between gate and source/drain terminal. During the measuring process, the samples remained in the bent state for at least 10 minutes and the strain has been applied parallel to the channel, i.e., to the current flow direction. The gate width W and length L of all transistors are 200 µm and 2 µm, respectively. The 12 nm ZTO channel exhibits a free-carrier concentration of 1.5×10^{18} cm^{-3} and a charge-carrier mobility of 7.5 $cm^2V^{-1}s^{-1}$. Respective transistor parameters derived from the transfer characteristics are given in **Figure 4B**. All MESFETs exhibit a current on/off ratio between six and seven order of magnitude and can be switched between on and off state within a similar gate voltage range of less than 2.5 V, attributed to their subthreshold swing of about 350 mV/dec. As expected, a clear

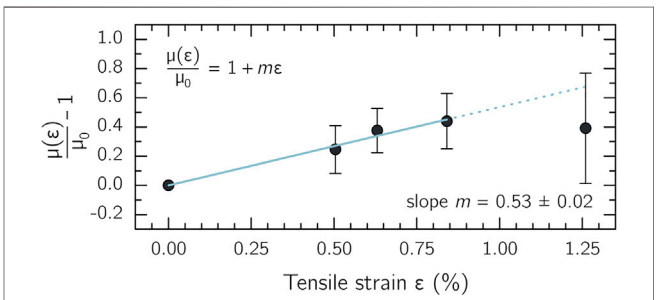

FIGURE 5 | Strain-dependence of the normalized field-effect mobilities calculated from the transfer characteristics of ZTO based MESFETs according to **Eq. 2**.

dependence of the channel conductivity on the tensile strain is observable, considering the doubling of the maximum on-current up to 0.3 mA. Consequently, the maximum transconductance improves from initially 109 µS to roughly 220 µS (ε = 1.26 %) for a bending radius of 2 mm. Further, the threshold voltage exhibits a distinct normally-on shift of about 150 mV toward negative gate voltages with increasing the tensile strain. A similar trend is observable for IGZO based transistors and originates from the increased channel conductivity under tensile strain (Münzenrieder et al., 2011; Petti et al., 2014). After reflattening the sample, the investigated MESFETs are fully operational and the negative V_T is reversed. The transistors show no visible cracks even after multiple tensile bending to radii of 2 mm. However, the unbent MESFETs exhibit a reduced

gate leakage current and thus an increase of the current on/off ratio to seven orders of magnitude as well as an improved subthreshold swing of 150mV/dec after the whole bending procedure.

Associated strain-dependent normalized field-effect mobilities calculated from the transfer characteristics using

$$\mu = \frac{L}{W}\frac{g_{max}}{end} \quad (2)$$

are shown in **Figure 5**, where g_{max}, e and d denote the maximum transconductance, the elementary charge and the channel thickness, respectively. As expected, the channel conductivity increases upon subjecting the devices to tensile bending stress and consequently, an improvement of the field-effect mobility of almost 80 % from 4.2 $cm^2V^{-1}s^{-1}$–7.5 $cm^2V^{-1}s^{-1}$ has been observed. According to Heremans *et al.*, the change of the charge-carrier mobility for moderate levels of mechanical strain can be described by $\mu(\varepsilon)\mu_0^{-1} = (1 + m\varepsilon)$, where $\mu(\varepsilon)$ and μ_0 corresponds to the mobility in bent and flat condition, respectively, and m denotes an empirical proportionality constant (Heremans et al., 2016). For tensile strain, ε is positive, whereas the sign of m certainly depends on the channel material itself. For amorphous oxide semiconductors such as IGZO based transistors, obtained m values are usually positive and have found to be ranging from +1.4 to +2.7 (Münzenrieder et al., 2013; Tripathi et al., 2015). Linear regression of the strain-dependent field-effect mobilities calculated for the presented ZTO MESFETs yields $m = 0.53 \pm 0.02$, indicating a less sensitive device operation under tensile bending compared to IGZO.

4 CONCLUSION

Amorphous ZTO thin-films have been investigated regarding their performance stability under strain induced by bending around radii ranging from 8 mm down to 1 mm. Force spectroscopy of bent ZTO samples yield no significant effect on the elastic properties of ZTO up to a tensile strain of 0.83 % ($R = 3$ mm). By exceeding that value, however, the ZTO thin-film starts to plastically deform. Additionally, the impact of residual compressive and tensile strain on the resistivity, the free-carrier concentration as well as the charge-carrier mobility of ZTO has been compared after the samples have been subjected to bending in between Hall-effect and conductivity measurements. Again, the electrical properties appear to be unaffected by the internal strain up to $\varepsilon = \pm 1.24$ % ($R = 2$ mm). Further increasing the tensile and compressive strain to 2.5 % causes the ZTO surface to become brittle and the resistivity to irreversibly increase by at least two orders of magnitude. Lastly, the operation of ZTO based MESFETs has been investigated while bending the sample around radii between 5 mm and 2 mm. Even up to highest applied tensile strain of 1.26 %, a reasonably stable device performance in terms of a current on/off ratio around six to seven orders of magnitude, a subthreshold swing of 350 mV/dec and a field-effect mobility as high as 7.5 $cm^2V^{-1}s^{-1}$ is observable. Gradually increasing the tensile strain results in a reversible negative V_T shift of approximately 150 mV as well as a steady improvement of the channel conductivity and consequently an increase of the field-effect mobility of almost 80 %. After reflattening the sample, the MESFETs are fully functional and no visible cracks across the transistor structures are observable.

To further improve the transistor performance stability for smaller bending radii, a device passivation or even full sample encapsulation, e.g., with polyimide in the order of the substrate thickness, should shift the neutral plane into the center of the transistor channel to minimize the total induced strain. Nevertheless, the presented results demonstrate a sufficient durability of amorphous ZTO and less sensitive device operation behavior compared to IGZO when being subjected to mechanical stress in terms of bending-induced compressive and tensile strain and thus render ZTO a promising candidate for future bendable electronic applications.

DATA AVAILABILITY STATEMENT

The raw data supporting the conclusions of this article will be made available by the authors, without undue reservation.

AUTHOR CONTRIBUTIONS

OL prepared the samples and performed the electrical characterization. MS conducted AFM measurements and assisted with data evaluation. OL drafted the manuscript; MS, HvW and MG helped discussing results, commented on the manuscript during its preparation and approved the final version.

FUNDING

Parts of this work have been funded by Deutsche Forschungsgemeinschaft within the framework of Schwerpunktprogramm SPP 1796 “High Frequency Flexible Bendable Electronics for Wireless Communication Systems (FFlexCom)” (Grant No. GR 1011/31-2). The authors further acknowledge support from Universität Leipzig within the program of Open Access Publishing.

REFERENCES

Billah, M. M., Hasan, M. M., and Jang, J. (2017). Effect of Tensile and Compressive Bending Stress on Electrical Performance of Flexible A-Igzo Tfts. *IEEE Electron. Device Lett.* 38, 890–893. doi:10.1109/led.2017.2707279

Cappella, B., and Dietler, G. (1999). Force-distance Curves by Atomic Force Microscopy. *Surf. Sci. Rep.* 34, 1–104. doi:10.1016/s0167-5729(99)00003-5

Dang, G. T., Kawaharamura, T., Furuta, M., and Allen, M. W. (2017). Zinc Tin Oxide Metal Semiconductor Field Effect Transistors and Their Improvement under Negative Bias (Illumination) Temperature Stress. *Appl. Phys. Lett.* 110, 073502. doi:10.1063/1.4976196

Fernandes, C., Santa, A., Santos, Â., Bahubalindruni, P., Deuermeier, J., Martins, R., et al. (2018). A Sustainable Approach to Flexible Electronics with Zinc-Tin Oxide Thin-Film Transistors. *Adv. Electron. Mater.* 4, 1800032. doi:10.1002/aelm.201800032

Heremans, P., Tripathi, A. K., de Jamblinne de Meux, A., Smits, E. C. P., Hou, B., Pourtois, G., et al. (2016). Mechanical and Electronic Properties of Thin-Film Transistors on Plastic, and Their Integration in Flexible Electronic Applications. *Adv. Mater.* 28, 4266–4282. doi:10.1002/adma.201504360

Hosono, H. (2018). How We Made the Igzo Transistor. *Nat. Electron.* 1, 428. doi:10.1038/s41928-018-0106-0

Jackson, W. B., Herman, G. S., Hoffman, R. L., Taussig, C., Braymen, S., Jeffery, F., et al. (2006). Zinc Tin Oxide Transistors on Flexible Substrates. *J. Non-Crystalline Sol.* 352, 1753–1755. doi:10.1016/j.jnoncrysol.2005.11.080

Jackson, W. B., Hoffman, R. L., and Herman, G. S. (2005). High-performance Flexible Zinc Tin Oxide Field-Effect Transistors. *Appl. Phys. Lett.* 87, 193503. doi:10.1063/1.2120895

Jain, A., Ong, S. P., Hautier, G., Chen, W., Richards, W. D., Dacek, S., et al. (2013). Commentary: The Materials Project: A Materials Genome Approach to Accelerating Materials Innovation. *APL Mater.* 1, 011002. doi:10.1063/1.4812323

Lahr, O., Bar, M. S., Wenckstern, H., and Grundmann, M. (2020). All-Oxide Transparent Thin-Film Transistors Based on Amorphous Zinc Tin Oxide Fabricated at Room Temperature: Approaching the Thermodynamic Limit of the Subthreshold Swing. *Adv. Electron. Mater.* 6, 2000423. doi:10.1002/aelm.202000423

Lahr, O., Vogt, S., Wenckstern, H., and Grundmann, M. (2019). Low-Voltage Operation of Ring Oscillators Based on Room-Temperature-Deposited Amorphous Zinc-Tin-Oxide Channel MESFETs. *Adv. Electron. Mater.* 5, 1900548. doi:10.1002/aelm.201900548

Lahr, O., von Wenckstern, H., and Grundmann, M. (2020). Ultrahigh-performance Integrated Inverters Based on Amorphous Zinc Tin Oxide Deposited at Room Temperature. *APL Mater.* 8, 091111. doi:10.1063/5.0022975

Lahr, O., Zhang, Z., Grotjahn, F., Schlupp, P., Vogt, S., von Wenckstern, H., et al. (2019). Full-swing, High-Gain Inverters Based on Znsno Jfets and Mesfets. *IEEE Trans. Electron. Devices* 66, 3376–3381. doi:10.1109/ted.2019.2922696

Lee, K., Kim, Y.-H., Kim, J., and Oh, M. S. (2018). Transparent and Flexible Zinc Tin Oxide Thin Film Transistors and Inverters Using Low-Pressure Oxygen Annealing Process. *J. Korean Phys. Soc.* 72, 1073–1077. doi:10.3938/jkps.72.1073

Münzenrieder, N., Cherenack, K. H., and Troster, G. (2011). The Effects of Mechanical Bending and Illumination on the Performance of Flexible Igzo Tfts. *IEEE Trans. Electron. Devices* 58, 2041–2048. doi:10.1109/ted.2011.2143416

Münzenrieder, N., Petti, L., Zysset, C., Kinkeldei, T., Salvatore, G. A., and Tröster, G. (2013). Flexible Self-Aligned Amorphous Ingazno Thin-Film Transistors with Submicrometer Channel Length and a Transit Frequency of 135 Mhz. *IEEE Trans. Electron. Devices* 60, 2815–2820. doi:10.1109/ted.2013.2274575

Petti, L., Münzenrieder, N., Salvatore, G. A., Zysset, C., Kinkeldei, T., Büthe, L., et al. (2014). Influence of Mechanical Bending on Flexible Ingazno-Based Ferroelectric Memory Tfts. *IEEE Trans. Electron. Devices* 61, 1085–1092. doi:10.1109/ted.2014.2304307

Salvadori, M. C., Brown, I. G., Vaz, A. R., Melo, L. L., and Cattani, M. (2003). Measurement of the Elastic Modulus of Nanostructured Gold and Platinum Thin Films. *Phys. Rev. B* 67, 153404. doi:10.1103/physrevb.67.153404

Schlupp, P., von Wenckstern, H., and Grundmann, M. (2013). Amorphous Zinc-Tin Oxide Thin Films Fabricated by Pulsed Laser Deposition at Room Temperature. *MRS Online Proc. Libr.* 1633, 101–104.

Schlupp, P., Schein, F.-L., von Wenckstern, H., and Grundmann, M. (2015). All Amorphous Oxide Bipolar Heterojunction Diodes from Abundant Metals. *Adv. Electron. Mater.* 1, 1400023. doi:10.1002/aelm.201400023

Schlupp, P., Vogt, S., von Wenckstern, H., and Grundmann, M. (2020). Low Voltage, High Gain Inverters Based on Amorphous Zinc Tin Oxide on Flexible Substrates. *APL Mater.* 8, 061112. doi:10.1063/1.5143217

Schlupp, P., von Wenckstern, H., and Grundmann, M. (2017). Schottky Barrier Diodes Based on Room Temperature Fabricated Amorphous Zinc Tin Oxide Thin Films. *Phys. Status Solidi A.* 214, 1700210. doi:10.1002/pssa.201700210

Townsend, P. H., Barnett, D. M., and Brunner, T. A. (1987). Elastic Relationships in Layered Composite media with Approximation for the Case of Thin Films on a Thick Substrate. *J. Appl. Phys.* 62, 4438–4444. doi:10.1063/1.339082

Tripathi, A. K., Myny, K., Hou, B., Wezenberg, K., and Gelinck, G. H. (2015). Electrical Characterization of Flexible Ingazno Transistors and 8-b Transponder Chip Down to a Bending Radius of 2 Mm. *IEEE Trans. Electron. Devices* 62, 4063–4068. doi:10.1109/ted.2015.2494694

Vogt, S., von Wenckstern, H., and Grundmann, M. (2018). Mesfets and Inverters Based on Amorphous Zinc-Tin-Oxide Thin Films Prepared at Room Temperature. *Appl. Phys. Lett.* 113, 133501. doi:10.1063/1.5038941

Conflict of Interest: The authors declare that the research was conducted in the absence of any commercial or financial relationships that could be construed as a potential conflict of interest.

Publisher's Note: All claims expressed in this article are solely those of the authors and do not necessarily represent those of their affiliated organizations, or those of the publisher, the editors and the reviewers. Any product that may be evaluated in this article, or claim that may be made by its manufacturer, is not guaranteed or endorsed by the publisher.